JOURNAL OF SPACECRAFT AND ROCKETS
Vol. 33, No. 4, July–August 1996

Solid-Rocket-Motor Contribution to Large-Particle Orbital Debris Population

Gregory W. Ojakangas*
University of Minnesota at Duluth, Duluth, Minnesota 55812-2496
B. Jeffrey Anderson†
NASA Marshall Space Flight Center, Huntsville, Alabama 35812
and
Phillip D. Anz-Meador‡
Viking Science and Technology, Inc., Houston, Texas 77058

Observations of solid-rocket-motor static firings indicate that these motors contribute to the centimeter-sized orbital debris population when they are used as launch vehicles. An analytic solution for the orbital distribution of this ablative debris from on-orbit solid-rocket-motor firings is presented and applied to a data set containing a large fraction of such firings in Earth orbit during the 1980s. Assuming 400 ablative objects are released per burn, it is found for altitudes above about 500 km that their spatial density is negligible in comparison with predicted 1-cm densities from other sources for the year 1990. Ablative-debris densities exceed predictions for other sources below about 250 km, but these densities are small. In the planned altitude range for the International Space Station (about 400 km), our results suggest that ablative particles pose about 10% as great a hazard as debris from other sources. However, these results are preliminary and should be updated as more complete data become available regarding the number of particles emitted per firing and historical solid-rocket-motor launches.

Nomenclature

dm/dt = rate of burn of fuel mass, kg/s
F = fraction of burn during which ablative particles are emitted, dimensionless
m_f = total initial fuel mass, kg
$m(t)$ = spacecraft mass as a function of time, kg
m_0 = dry mass of solid rocket motor, kg
$N_d(r)$ = number of ablative objects emplaced within apse-radius increment dr, per increment dr, dimensionless
n_d = number of ablative particles emitted by time t, dimensionless
n_{d0} = total number of ablative particles emitted per burn, dimensionless
r_e = radius of the Earth
r_{sc} = new spacecraft apse radius resulting from burn
r_0 = radius of original orbit apse at which burn takes place, m
r_{00} = radius of original orbit apse at which burn does not take place, m
v = spacecraft velocity
v_{co} = velocity of object in circular orbit of radius r_0
v_{ex} = exhaust velocity, m/s
Δv_d = velocity of ablative debris relative to spacecraft rest frame before burn, m/s
Δv_{sc} = total velocity change imparted to spacecraft during burn, m/s

Introduction

SOLID rocket motors (SRMs) are frequently employed at orbital altitudes as the final stage of satellite launch systems. They are either used as launch vehicles or occasionally built directly into the satellite itself. Examples include the Inertial Upper Stage (IUS), the PAM-D, the U.S. Scout and Pegasus vehicles, STAR-series rockets, the Japanese MU-3S, and the Indian SLV-3. In this paper, we examine the possible effects on the orbital debris environment of particles, typically in the centimeter size range, that are emitted by SRMs during their operation. We first describe results from observations of debris generated during actual SRM test firings. We then provide an analysis, based on the usage of solid motor upper stages during the 1980s, of their possible contribution to the orbital debris population during that time period.

Solid Motors as a Source of Large Fragments

A variety of observations indicate that numerous low-velocity debris fragments are generated during SRM burns. With characteristic major diameters of about 1 cm, these particles are large in relation to the ~1-μm particle size typical in the bulk of the effluent, and they are slow in the sense that they are emitted at speeds much lower than that of the SRM exhaust particles. Because of their size, these particles may pose a significant threat to space-vehicle structures. Nonetheless, prior to the present study, we are unaware of any concerted attempt to characterize large orbital debris fragments generated by SRMs.

Two examples of partial measurements of production rates of large fragments during solid-motor tests performed at the Marshall Space Flight Center (MSFC) are provided in Fig. 1. Figure 1a shows the number of fragments observed per second on a high-speed video of a STAR-63 test firing. The motor burned for 97 s while spinning in a horizontal orientation at 33 rpm about the nozzle axis. Data were taken from a high-speed video of the SRM nozzle and a portion of the exhaust plume. The fragments were observed to leave the nozzle at a high angle to the primary flow, both above and below the main plume. No fragments were visible in front or behind the plume because of the brightness of the flow—so the total number of fragments produced were not counted. The smallest particles observable on film in this case are estimated to be about 1 cm in diameter. Figure 1b shows similar data extracted from high-speed films of two nocturnal solid propulsion test bed (SPTB) firings at the MSFC. These burns are nozzle up static firings of 48-in. motors, each approximately 30 s in duration, conducted to test motor materials and construction features. The films were taken at 1000 frames per second by cameras arranged so as to view the entire plume at once.

Received June 26, 1995; revision received Feb. 27, 1996; accepted for publication Feb. 27, 1996.

*Assistant Professor, Department of Geology, 10 University Drive.
†Aerospace Engineer, Electromagnetic and Aerospace Environments Branch, Mail code El54.
‡Principal Scientist, 16821 Buccaneer Lane, Suite 206.

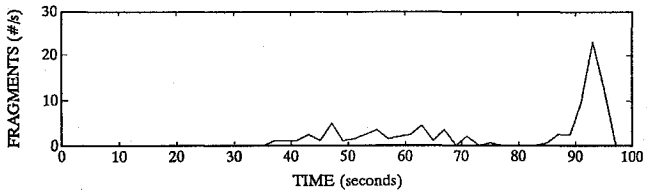

a) STAR-63 motor, horizontal firing

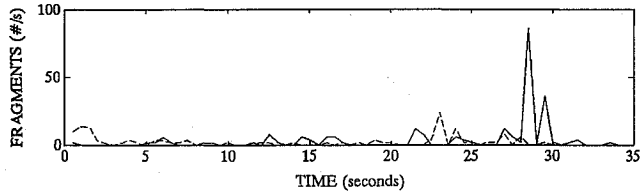

b) SPTB motors, vertical firings

Fig. 1 Fragment production during SRM test firings.

Fig. 2 Char fragment from SPTB motor firing.

Because of this arrangement, the smallest particles observable on film in this case are several centimeters in diameter. Most fragments observed were carried up with the plume, becoming visible as they exited the plume at the side or top. It is clear from Figs. 1a and 1b that most fragments tend to be ejected during the second half of the burn, with a substantial pulse at the end. Total particle counts from each of the curves in the figure range roughly between 100 and 200.

The quantity and physical properties of these fragments are not easily determined. The production is believed to be dependent on the test configuration—whether the nozzle is oriented up, down, or horizontally, the motor spin rate, etc.—and varies from test to test even for duplicate motors in the same test configuration. This is evident from examining the motor casings following tests, and is to be expected from the complex hydrodynamic flows in the motor interior during the burn.

For one SPTB test, half a dozen collection pads were deployed in the area around and downwind of the test motor. The pads consisted of tarps in square frames approximately 1 m on a side, filled with water. The spacing between pads was too great, and the number of pads too few, to provide quantitative data on fragment numbers. However, 12 fragments with cross-sectional areas over 10 mm^2 were caught on one pad, 3 were caught in another, and a number were retrieved from the surrounding grass. Figure 2 shows a photograph of a thin, fragile piece of char about 2 mm thick and roughly 5 cm in longest dimension. A number of similar fragments were found in the field surrounding the test fixture following the firings. A few kilograms of similar material is typically found loose in the motor casing upon disassembly following these tests. The intact portions of the motor's internal structure—inhibitors, insulation, and nozzle—show obvious signs of erosion, delamination, and mechanical damage, all of which is considered normal.

Production Mechanisms

Some potential sources of the large debris described above can be understood by considering a typical orbital-insertion SRM. Because of the high performance requirements for such motors, fine powdered aluminum is currently the fuel of choice. This is mixed with an oxidizer, usually ammonium perchlorate, and a binder material such as carboxyl- or hydroxyl-terminated polybutadiene. The binder holds the aluminum and ammonium perchlorate powders together and imparts the basic rheological and structural properties of the propellant casting. The Orbus-6, for example, contains 2700 kg (6000 lb) of propellant composed of 68% ammonium perchlorate, 18% aluminum, and 14% binder and additives. During steady-state motor firing, the aluminum is oxidized and ejected from the nozzle in the form of fine (<10-μm diam) droplets and particles. Because of their small size and short orbital lifetime, these particles do not contribute significantly to the debris accumulation problem. Their effects on spacecraft are limited to surface erosion and window pitting. Several production mechanisms for large debris from solid-motor burns are possible. The relative importance of each is unknown at this time, and it probably depends greatly on the motor design. The following mechanisms are probably the most significant:

1) Deterioration of internal motor structure from the thermal and fluid-dynamical forces. Selection of materials for the inhibitors, insulation, nozzle, or other internal components which will maintain structural integrity while exposed to the intense heat and pressure in the motor during the burn is always a key issue in the design and development of any SRM system. Attention to this concern during construction helps minimize structural materials as a debris source, but the observations previously described imply it is still a probable source.

2) Loose fragments of unburned propellant resulting from uneven burning. During the burn the propellant grain is consumed and gradually recedes to the motor liner. If the motor design and construction are optimal, all the propellant is consumed, leaving no component behind to break loose and be ejected from the motor.

3) Aluminum oxide slag generated during the steady motor burn. The mass fraction of aluminum oxide in SRM exhaust is about 30%. Internal-flow calculations[1,2] indicate that a small portion of this aluminum oxide does not flow directly out the nozzle, but rather impinges on the inner surface of the motor and runs down the surface toward the nozzle. SRM nozzles are generally re-entrant, i.e., they protrude into the combustion chambers. This design minimizes the length of the motor, but it also creates a toroidal pocket surrounding the nozzle entrance where the aluminum oxide accumulates in a slag pool. Axial acceleration due to motor thrust and centrifugal force due to motor spin, typically 30–90 rpm, enhance the accumulation of slag. Slag deposits are routinely found in SRMs during posttest inspection. Real-time x-ray radiography taken during motor firings reveals slag accumulating around the periphery of the nozzle entrance, periodically spilling over into the nozzle. Occasionally small spikes appear in the chamber pressure, which could be attributed to the passage of slag through the nozzle. The tremendous aerodynamic shear forces in the nozzle tend to disrupt the slag into small fragments. Little is known about the total mass and size distribution of the slag ejecta. Since the slag pool forms early in the motor burn, some of the aluminum oxide generated in the combustion chamber exits the motor in this highly nonideal fashion.

4) Expulsion of slag and material fragments during the final moments of the burn. After the propellant is consumed, the motor sometimes continues to outgas significantly as the liner and insulator char. Chamber pressures can remain high enough to lead to unwanted residual thrust. As the burn terminates, this slight residual thrust will certainly help to expel particles that are not highly sheared, and thus typically larger than particles emitted well before shut down. In addition, slag samples collected from motors following a firing tend to show a porous structure, indicating that they contain substantial trapped gas when they solidify. Expansion of this trapped gas during this depressurization phase (before complete shutdown) can be expected to break and separate slag fragments from the residual pool, leading to their ejection from the motor.

In light of their probable production modes discussed earlier, we hereafter refer to the large debris particles produced by SRMs

as ablative objects. In the following section, this term serves to distinguish this debris from the much smaller and faster-moving exhaust particles.

Analysis

To estimate the SRM contribution to the total orbital debris population, we first derive an expression for the distributions of orbital apses for ablative objects emitted during a single SRM burn. We then derive the resulting spatial distribution of the debris using the method of Kessler.[3] Finally, we add together the predicted debris densities resulting from 108 SRMs launched during the 1980s and compare this sum with the total predicted debris density, from NASA's orbital-debris-environment simulation program known as EVOLVE, at the end of 1990.

For the analysis, we assume a simple model of the source term based on the observations discussed. We assume that 400 spherical objects of 1.5-cm diam are emitted during each SRM burn. This number is taken to be somewhat larger than the totals of Fig. 1 as a first attempt to allow for the viewing-geometry limitations during the test firings (see Introduction). The release is assumed to occur at a uniform rate for a specified fraction of the total burn duration, with a retrograde velocity of 75 m/s with respect to the vehicle. The presented results are insensitive to the magnitude of this velocity, which should be true as long as it is small relative to the spacecraft velocity. The radial component of velocity (normal to the direction of travel) is ignored. We also consider the case where half of the objects are released at the completion of the burn.

Apse Density from a Single SRM Burn

Our analysis is simplified by the following assumptions, all of which are nearly always true: 1) SRM burns are of short duration relative to an orbit period, 2) they are performed when the SRM is at one apse of some defined initial orbit, and 3) the thrust is oriented horizontally. Under these conditions, the orbital radius of the apse at which the burn occurs remains the radius of one of the apsides of the final orbit—the burn only changes the radius of the opposite apse. We also assume that the debris objects are emitted at a uniform rate throughout some fraction F of the burn time preceding motor cutoff. Under these assumptions, the distribution of apse heights of the ablative objects can be easily calculated analytically, beginning from the equation of motion for a rocket fired horizontally (i.e., in the absence of a body force acting along its direction of motion):

$$m(t)\frac{\mathrm{d}v}{\mathrm{d}t} = v_{\mathrm{ex}}\frac{\mathrm{d}m}{\mathrm{d}t} \tag{1}$$

where

$$m(t) = (m_0 + m_f) - \frac{\mathrm{d}m}{\mathrm{d}t}t \tag{2}$$

Inserting Eq. (2) into Eq. (1) and integrating with respect to time yields the spacecraft velocity, relative to its value just before the burn, as a function of time:

$$v(t) = -v_{\mathrm{ex}}\,\ell n\left[1 - \frac{(\mathrm{d}m/\mathrm{d}t)t}{m_0 + m_f}\right] \tag{3}$$

If the ablative particles are emitted uniformly over the final fraction F of the burn time, the following relationship may be used to replace time by the number of debris objects that have been emitted by time t:

$$\frac{n_d}{n_{d0}} = \frac{(\mathrm{d}m/\mathrm{d}t)t - m_f(1-F)}{m_f F} \tag{4}$$

Solve Eq. (4) for $(\mathrm{d}m/\mathrm{d}t)t$ and insert the result into Eq. (3). By subtracting the relative velocity v_d of the ablative objects from the resulting expression, we obtain the velocity of ablative debris relative to the rest frame of the spacecraft just before the burn:

$$\Delta v_d = -v_{\mathrm{ex}}\,\ell n\left[1 - \frac{m_f F(n_d/n_{d0}) + m_f(1-F)}{m_0 + m_f}\left(\frac{n_d}{n_{d0}}\right)\right] \tag{5}$$

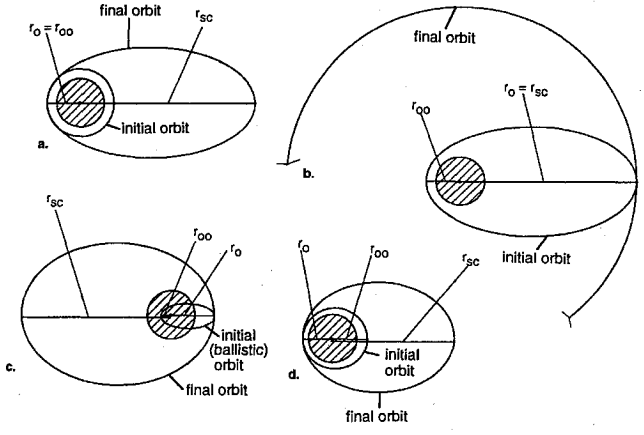

Fig. 3 Orbit configuration sketches for various SRM applications, not drawn to scale: a) GTO vehicles; b) geostationary spacecraft; c) SCOUT, SLV-3, and MU-3S launch vehicles; and d) final stage of EXOS-D rocket body.

Because of the assumption that the burn occurs quickly and is applied horizontally, all of the ablative particles have either pericenter or apocenter at the apse of the original orbit where the burn takes place. For the ablative debris orbits, the radius of the apse that is not located at r_0 is easily shown to be related to the velocity Δv_d by the equation

$$\Delta v_d = v_{\mathrm{co}}\left\{[2r/(r_0 + r)]^{\frac{1}{2}} - b\right\} \tag{6}$$

where

$$b \equiv \left(\frac{2r_{00}}{r_0 + r_{00}}\right)^{\frac{1}{2}}$$

Figure 3 is a sketch of various possible configurations of the spacecraft orbit before and after the burn. Solving for n_d in Eq. (5), replacing Δv_d by Eq. (6), and differentiating the result with respect to r gives the density of ablative-object orbital apses per unit radius:

$$N_d(r) = \frac{n_{d0}}{\sqrt{2F}}\left(\frac{m_0 + m_f}{m_f}\right)\frac{v_{\mathrm{co}}}{v_{\mathrm{ex}}}\exp\left(\frac{bv_{\mathrm{co}} - v_d}{v_{\mathrm{ex}}}\right)$$
$$\times\left[\exp\left(-\frac{v_{\mathrm{co}}}{v_{\mathrm{ex}}}\sqrt{\frac{2r}{r_0 + r}}\right)\frac{r_0}{(r_0 + r)^{\frac{3}{2}}r^{\frac{1}{2}}}\right] \tag{7}$$

This density applies only within a range of r values between r_1 and r_2, where

$$r_1 = A_1 r_0/(2 - A_1)$$
$$A_1 = \left\{\left(b - \frac{v_d}{v_{\mathrm{co}}}\right) - \frac{v_{\mathrm{ex}}}{v_{\mathrm{co}}}\,\ell n\left[1 - \frac{m_f}{m_0 + m_f}(1-F)\right]\right\}^2 \tag{8}$$
$$r_2 = \frac{A_2 r_0}{2 - A_2}, \qquad A_2 = \left(b + \frac{\Delta v_{\mathrm{sc}} - v_{\mathrm{d}}}{v_{\mathrm{co}}}\right)^2$$

These values were obtained by replacing the left-hand side of Eq. (6) by the smallest and largest velocities imparted to ablative debris during the burn, namely $-v_d$ and $\Delta v_{\mathrm{sc}} - v_d$, and solving for r. The change Δv_{sc} may be written in terms of r_{sc} using Eq. (6):

$$\Delta v_{\mathrm{sc}} = v_{\mathrm{co}}\left(\sqrt{\frac{2r_{\mathrm{sc}}}{r_0 + r_{\mathrm{sc}}}} - b\right) \tag{9}$$

In this development, the final apse radii of the SRM orbit are r_0 and r_{sc}. Since one apse is necessarily at $r = r_0$ for all objects, Eqs. (7) and (8) complete the description of the apogee and perigee distributions for ablative debris from a single SRM burn, or equivalently, the

semimajor axis and eccentricity distributions of the debris. Note that the distribution does not depend on the rate of mass loss during the burn, dm/dt. This result is as one would expect if the burn takes place very quickly relative to an orbit period.

It is also useful to relate the total fuel mass m_f to the final orbit of the SRM using Eqs. (3) and (9):

$$\frac{m_f}{m_0} = \exp\left[\frac{v_{co}}{v_{ex}}\left(\sqrt{\frac{2r_{sc}}{r_0 + r_{sc}}} - b\right)\right] - 1 \qquad (10)$$

With the aid of Eq. (10), it may be shown analytically that

$$\int_{r_1}^{r_2} N_d(r)\,dr = n_{d0} \qquad (11)$$

Application to Individual Solid Rocket Motors

In this section, we apply the results of the preceding analysis to several individual historical SRM launches, assuming that half of the ablative particles per firing are emitted uniformly throughout the second half of the burn, and that half are emitted at the end of the burn. In each of the following examples, the former is treated using $F = 0.5$, and the latter is approximated by $F = 0.001$.

We first consider the ablative debris distribution from the first stage of the IUS vehicle employed to launch the Galileo spacecraft. Galileo was deployed atop the IUS two-stage booster released from the Space Shuttle Atlantis on Oct. 18, 1989, in a circular orbit of altitude 300 km and inclination 34.3 deg. The circular orbit radius thus became the perigee radius of the final orbit. The first-stage burn raised the apogee of the IUS to 25,600-km altitude. This orbital configuration is like that of Fig. 3a. The second stage carried Galileo into a heliocentric orbit. Figure 4a shows the apse distribution of the ablative particles from the first stage that are emitted uniformly through the second half of the burn. The apse density for the particles emitted at the end of the burn is not shown. It would be described by a delta function at the right end of the density curve. The Galileo IUS upper-stage burn configuration corresponds to $r_0 = r_{00} = r_e + 300$ km, and $r_{sc} = r_e + 25{,}600$ km. To obtain this distribution, the only pieces of information required (in addition to the parameter values assumed in the above analysis) are the initial and final orbits of the stage, and the exhaust velocity. We assume throughout this report that $v_{ex} = 2.7$ km/s, a value appropriate for SRM propellant. Note that with Eqs. (7) and (10) and the current assumptions, the orbital distribution of ablative debris is independent of the actual dry mass of an SRM. If the initial and final orbits of the SRM are known, m_0 cancels out of the equations.

Debris orbital elements may be transformed into effective spatial densities as functions of altitude using the equations given by Kessler.[3] For this work, the element distributions given above were integrated analytically over apse-height bins of 50-km width, and the results were transformed using these equations.

The solid curve of Fig. 4b shows the spatial density resulting from the distribution of Fig. 4a (with the particles emitted at the very end of the burn included). Also shown are the spatial densities corresponding to the assumptions that the ablative debris are emitted uniformly throughout the burn (dotted curve), and that all are emitted entirely at the end of the burn (dashed curve). Note that as the debris is emitted later in the burn, the resulting spatial density is decreased at low altitudes and increased at high altitudes.

The IUS solid rocket motor is but one of several vehicles that are typically fired in circular orbits so as to raise the apogee altitude while maintaining the perigee altitude roughly constant. This configuration is typical of SRM stages that are fired into geosynchronous transfer orbits (GTOs). In this configuration, they are often referred to as perigee-kick motors.

Solid rocket motors are also used for circularization of transfer orbits at the middle (20,000 km) or geosynchronous (roughly 36,000 km) altitude. When used in this manner, they are termed apogee-kick motors, because the burn occurs at the apogee of a GTO orbit. Generally, a prior stage of the same vehicle performs a perigee-kick burn to attain transfer orbit from an initial circular orbit at an altitude of a few hundred kilometers, and the apogee-kick burn is performed by the subsequent stage, leaving the spacecraft in its operational orbit. This orbital configuration is sketched in Fig. 3b.

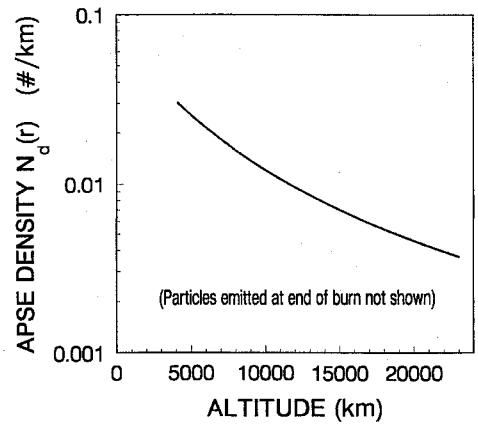

Fig. 4a Apse density of ablative particles from the IUS vehicle used to launch the Galileo spacecraft.

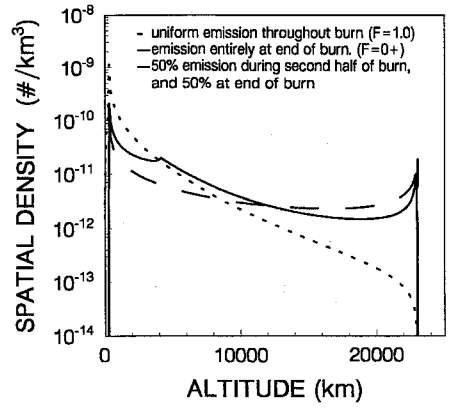

Fig. 4b Initial spatial density of ablative debris from Galileo IUS.

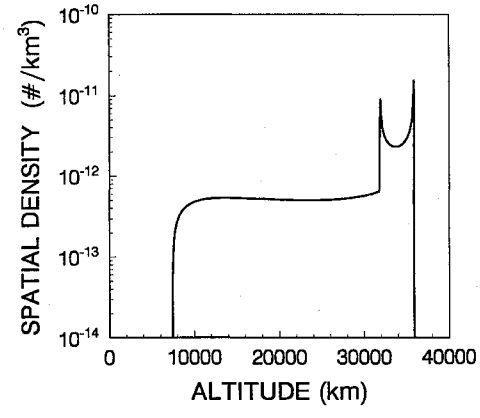

Fig. 5 Initial spatial density of ablative debris from a typical circularization burn at geostationary altitude: the second stage of the USA 48 rocket body.

An example of this burn configuration is given by the USA 48 SRM vehicle, launched in November 1989. The two-stage IUS system was used for this launch as well. The first stage attained a GTO orbit with perigee and apogee at 210- and 35,862-km altitude, respectively. The second stage performed an apogee-kick burn and circularized its orbit at 35,862 km. The second-stage burn is thus defined by $r_{sc} = r_0 = r_e + 35{,}862$ km, and $r_{00} = r_e + 210$ km. Figure 5 shows the model results for the spatial density of the ablative debris from the second stage. The particles emitted at the end of the burn dominate the spatial density at high altitudes, as is clearly visible in the figure. These particles occupy essentially a single orbit, which exhibits sharp spatial density maxima at perigee and apogee.

A class of smaller, less powerful SRMs contributes very importantly to the low-Earth-orbit ablative-debris population. This class is largely composed of the American Pegasus and Scout, the Japanese MU-3S, and the Indian SLV-3 launch systems. These are multistage launch systems that lift relatively small payloads into low Earth orbit. They are all similar in that generally the penultimate stage achieves a velocity of about 5 km/s, at which point the final stage is fired. Thus, the trajectory of the penultimate stage is ballistic, and only the final stage achieves orbit.[4] Given the postburn orbit of the final stage of one of these spacecraft, we can generally estimate the preburn perigee radius r_{00} by assuming that the velocity was $v_p = 5$ km/s (horizontal) just before the burn, and that the burn occurred at the perigee of the postburn (final) orbit. The expression is

$$r_{00} = \frac{cr_0^2}{1 - cr_0}$$

where

$$C \equiv \frac{v_p^2}{2GM} \tag{12}$$

and where G and M are the gravitational constant and the mass of the Earth. A sketch of the preburn and postburn trajectories for a final stage of one of these vehicles is given in Fig. 3c. One example from this class is the NOVA-11 launch vehicle, a Scout. The final stage of NOVA-11 achieved an orbit with perigee and apogee altitudes of 310 and 941 km, respectively. Thus, we have $r_0 = r_e + 310$ km and $r_{sc} = r_e + 941$ km. Using the assumptions described above, Eq. (12) gives $r_{00} = 4611$ km, implying that the penultimate stage trajectory was deeply ballistic. Figure 6 shows the predicted spatial density of ablative debris from this rocket body. Most of the particles emitted during the second half of the burn have perigees well below the surface of the Earth, so most re-enter within one orbit period. However, recall that half of the particles are assumed to be emitted at the end of the burn. These particles do not re-enter immediately and are responsible for most of the spatial density shown in Fig. 6.

Yet another configuration for the preburn and postburn orbits is exemplified by the EXOS-D spacecraft launch. The vehicle used in this case was the Japanese MU-3S II rocket, a more powerful successor to the MU-3S system, for which the penultimate as well as the final stage is able to achieve orbital velocities. The penultimate stage achieved perigee and apogee altitudes of 270 and 567 km, respectively. The final burn was performed at perigee, raising the apogee of the final stage to 9816 km. Thus, to calculate the ablative debris distribution from the final-stage burn, we have $r_0 = r_e + 270$ km, $r_{00} = r_e + 567$ km, and $r_{sc} = r_e + 9816$ km. This configuration is sketched in Fig. 3d. Figure 7 shows the spatial density resulting from the final-stage burn. Because the preburn trajectory was already orbital, all of the ablative particles also have initially orbital trajectories. The peak in density at 8900 km represents the apogees of the objects emitted at the end of the burn, the peak at 2900 km represents the apogees of the particles emitted near the beginning of the second half of the burn, and the peak at 270 km results from the fact that all of the ablative particles have perigees at that altitude.

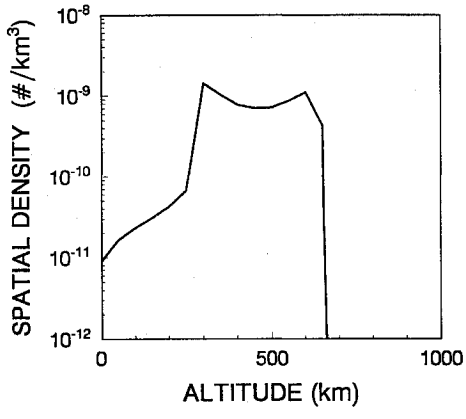

Fig. 6 Initial spatial density of ablative debris from a typical SCOUT launch vehicle: the final stage of the NOVA 11 rocket body.

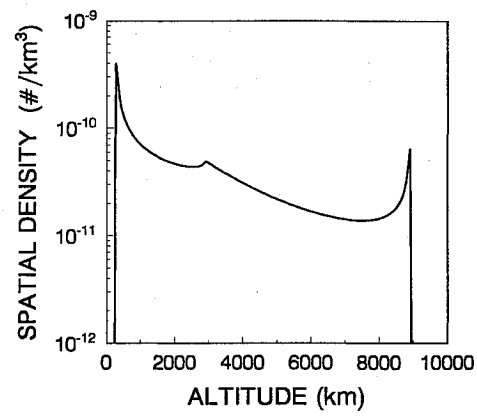

Fig. 7 Initial spatial density of ablative debris from the EXOS-D final stage. See text.

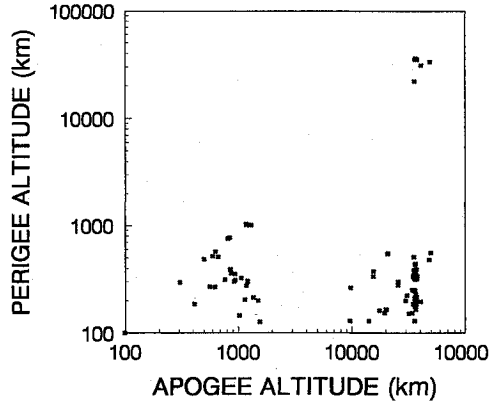

Fig. 8 Scatterplot of (apogee, perigee) pairs for SRMs launched during the 1980s.

Application to an Ensemble of Historical Launches

The preceding development was applied to a database containing the final orbits of 108 solid rocket motors launched in the 1980s. This database comprised essentially all SRMs launched during that decade that were not housed with the active payload. Preburn orbit configurations were derived from postburn orbits of previous stages where possible, or from the launch-vehicle type and the assumptions described in the previous section.

Figure 8 shows a scatterplot of the final orbit apogees and perigees of these SRMs. Most of the objects with apogees below 10,000 km are of the lighter class of launch vehicle described above (Scout, MU-3S, or SLV-3), and those with apogees above 10,000 km are of the heavier class (PAM-D, SGS II, IUS, or other STAR-class). Note the concentrations of rocket bodies in GTO and geostationary orbits. Also note that in this data set there are many more objects in GTO than in the geostationary orbit region, in spite of the fact that most rocket bodies in GTOs participated in delivering payloads into the geostationary region. The reason is that most of the geosynchronous Earth orbit (GEO) objects that the GTO rocket bodies delivered had their SRMs housed with the final active payload, so they were not included in the data set. To make up for this deficiency, those GTO objects that did not have explicit GEO counterparts in the data set were given them artificially by the computer code. These artificial GEO objects were assumed to attain circular orbits at the apogee altitude of the relevant GTO objects.

To include atmospheric drag in the development, the fast orbit propagation program DECAY was interfaced with the code that was developed to implement the theory described in the preceding sections. The DECAY program uses the analytic theory of orbit decay in an atmosphere[5] combined with a form of first-order perturbation theory to allow for the effects of lunisolar perturbations.[6] Simulations were performed assuming an ablative debris density of 3.5 g/cm^3, typical of porous aluminum oxide, and separate simulations were performed using a density of 1.8 g/cm^3, typical of the materials used for SRM thermal insulation. The orbits of the ablative particles were thus evolved over time, from the dates of the

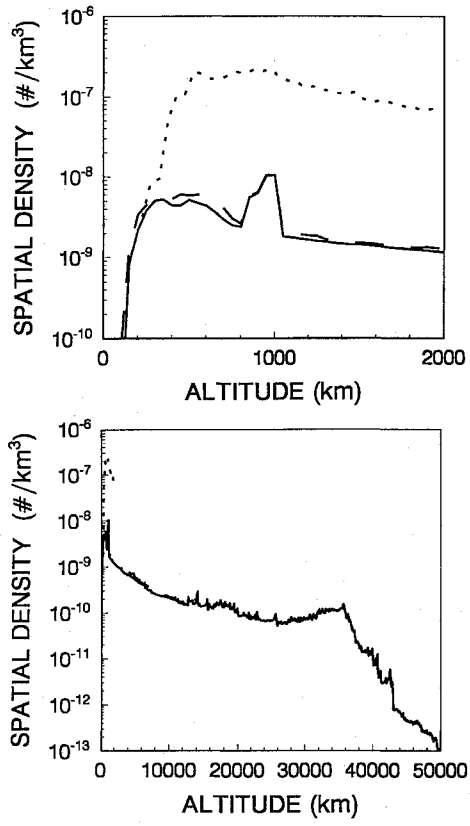

Fig. 9 Spatial densities, at the end of 1990, of ablative debris from SRMs launched during the 1980s.

SRM burns to the end of the year 1990, in discrete apogee–perigee bins of 50 km width. Yearly averaged historical solar flux values were employed in the computations, using the Jacchia–Lineberry atmospheric model.[7]

Figures 9a and 9b show the results of the computations. For comparison, an average 1-cm cumulative spatial density predicted by NASA's debris environment simulation code EVOLVE is also shown. Comparison with the results of similar computations with atmospheric drag removed reveals that drag reduces the predicted ablative particle densities at altitudes of several hundred kilometers by a factor of about 5–6 (more for the cases with the lower particle density of 1.8 g/cm^3) in all of the cases presented, over the 10-year period. This large an attenuation may appear somewhat surprising at first sight, because the most common SRM firings in the 1980s were of the type where the final orbit of the rocket body was a GTO. As one would expect, these firings produce many ablative particles with apogees well above 10,000 km (like those of most of the SRM final orbits) and perigee altitudes of a few hundred kilometers. These orbits may require well over 100 years to decay. However, as Fig. 4a illustrates, most of the ablative particles emitted during insertion of an SRM into such a final orbit have apogees of only several thousand kilometers, and these orbits characteristically decay in well under 10 years. Furthermore, a considerable percentage of the SRM firings in the 1980s were performed by the smaller class of these rockets, and most of the debris from these firings decays relatively quickly.

The spatial densities of ablative debris are less strongly reduced by atmospheric drag at higher altitudes, in general. It is because of this fact that the curves describing the results for the two choices of ablative particle densities are essentially coincident at high altitudes (see Fig. 9b). It is also interesting to note that the ablative particle density exceeds that predicted by EVOLVE for altitudes below 250–300 km, although the densities are about an order of magnitude smaller than the EVOLVE densities at altitudes appropriate to the International Space Station (about 400 km). Thus, the relative importance of the ablative debris hazard to the space station depends strongly on its proposed altitude. The enhanced density at low altitudes is caused by a rain of ablative particle orbits decaying from above.

Under the assumptions inherent in the model presented here, a space station of about 1000-m^2 surface area, operating at an altitude of about 400 km, would have roughly a 10% chance of suffering a hit by an ablative 1-cm particle in 30 years of operation, assuming that the densities shown for 1990 are indicative of those the space station experiences during its lifetime. This is about a factor of 10 smaller than the predicted 1-cm debris hazard resulting from other sources. However, three important points must be considered before judging the importance of the ablative-debris hazard: 1) the data set used in this analysis does not contain the SRMs launched before 1980 or after 1990, 2) it does not contain a large number of SRMs that are built into satellite hardware, and 3) the number of ablative particles per SRM burn used in this analysis represents our best estimate: the actual number is not well known. Unfortunately, this number is not easily refined because of the variability of the production processes and the expected sensitivity to the firing configuration. Ablative-particle production may be much different in the space environment than on the test stand. Radar observations of on-orbit firings are probably required to provide more accurate estimates. If ablative debris does prove to pose a significant problem for space missions, it will be helpful to carefully select launch dates and locations to take advantage of solar and lunar perturbations that can minimize the lifetime of the debris orbits.[8]

Conclusions

The observations of SRM test firings reported here clearly indicate that during burn these motors typically produce at least several hundred debris particles with diameters in the centimeter size range. Our estimates of the spatial debris densities in Earth orbit resulting from the use of SRMs as launch vehicles suggest that ablative debris may constitute a very important component of the centimeter-sized orbital debris environment. Preliminary results give an ablative debris hazard that is about 10% as great as that generated by other sources in the proposed altitude range for the International Space Station. However, these results need to be quantified with better data as discussed in this paper. Consideration of additional data could cause the predicted SRM densities to increase. Clearly, additional work is required before the importance of SRM debris to the total orbital debris environment can be firmly established.

Acknowledgments

The authors express gratitude to Donald J. Kessler of the NASA Johnson Space Center; Bob Reed and Michael Anderson of Sverdrup Technology, Inc., Arnold Air Force Base; and the personnel of the Propulsion Test Division and the Solid Motor Design Branch at NASA Marshall Space Flight Center for their support, references, and technical insights into the issues discussed here.

References

[1]Haloulakos, V. E., "Slag Mass Accumulation in Spinning Solid Rocket Motors," *Journal of Propulsion and Power*, Vol. 7, No. 1, 1991, pp. 14–21.

[2]Hess, E., Chen, K., Acosta, P., Brent, D., and Fendell, F., "Effect of Aluminized Grain Design on Slag Accumulation," *Journal of Spacecraft and Rockets*, Vol. 29, No. 5, 1992, pp. 697–703.

[3]Kessler, D. J., "Derivation of Collision Probability Between Orbiting Objects: The Lifetimes of Jupiter's Outer Moons," *Icarus*, Vol. 48, No. 1, 1981, pp. 39–48.

[4]Isakowitz, S. J., *International Reference Guide to Space Launch Systems*, AIAA, Washington, DC, 1991.

[5]King-Hele, D., *Theory of Satellite Orbits in an Atmosphere*, 1st ed., Butterworths, London, 1964.

[6]Mueller, A. C., "The Decay of the Low Earth Satellite," Lockheed Engineering and Sciences Co., Rept. 17520, Dec. 1981.

[7]Mueller, A. C., "Jacchia–Lineberry Upper Atmosphere Density Model," NASA Rept. 82-FM-52, JSC-18507, Oct. 1982.

[8]Siebold, K. H., Matney, M. J., Ojakangas, G. W., and Anderson, B. J., "Risk Analysis of 1–2 cm Debris Populations from Solid Rocket Motors and Mitigation Possibilities for GEO-Transfer Orbits," *Proceedings of the First European Conference on Space Debris* (ESA SD-01), edited by W. Flury, European Space Agency, Paris, 1993, pp. 349–354.

A. L. Vampola
Associate Editor